Rate of photon production in the quark-gluon plasma from lattice QCD

Marco Cè[1,2] Tim Harris,[3] Harvey B. Meyer[1,4] Aman Steinberg,[4,5] and Arianna Toniato[4]

[1]*Helmholtz-Institut Mainz, Johannes Gutenberg-Universität Mainz, D-55099 Mainz, Germany*
[2]*Theoretical Physics Department, CERN, CH-1211 Geneva 23, Switzerland*
[3]*Dipartimento di Fisica, Università di MilanoBicocca, and INFN, sezione di MilanoBicocca,*
Piazza della Scienza 3, I-20126 Milano, Italy
[4]*PRISMA⁺ Cluster of Excellence and Institut für Kernphysik, Johannes Gutenberg-Universität Mainz,*
D-55099 Mainz, Germany
[5]*Fakultät für Physik, Universität Bielefeld, D-33615 Bielefeld, Germany*

We calculate the thermal rate of real-photon production in the quark-gluon plasma at a temperature of $T = 254$ MeV using lattice QCD. The calculation is based on the difference between the spatially transverse and longitudinal parts of the polarization tensor, which has the advantage of falling off rapidly at large frequencies. We obtain this linear combination in the time-momentum representation from lattice QCD with two flavors of quarks in the continuum limit with a precision of about two parts per mille. Applying a theoretically motivated fit ansatz for the associated spectral function, we obtain values for the photon rate that are in line with QCD weak-coupling calculations. A representative result is $d\Gamma(k)/dk = (1.5^{+2.1}_{-1.5}) \cdot (10 \text{ fm})^{-4} \cdot (0.2 \text{ GeV})^{-1}$ at $k = 1.2$ GeV for the differential rate of photon production per unit volume of plasma.

I. INTRODUCTION

Strongly interacting matter undergoes a phase transition at a temperature of about 150 MeV [1–3]. Below the transition, the thermal medium is characterized by hadrons (nucleons, pions, kaons, …) as primary degrees of freedom, while well above the transition it is characterized by quarks and gluons, the elementary degrees of freedom of quantum chromodynamics (QCD). The high-temperature phase, the quark-gluon plasma (QGP), is probed experimentally in high-energy heavy-ion collisions at $T \lesssim 500$ MeV [4]. One of the remarkable properties of the medium is its ability to exhibit collective effects in spite of the rapid expansion occurring in heavy-ion collisions. The most prominent such effect is the large anisotropic flow observed in heavy-ion collisions at RHIC and the LHC, pointing to a small shear viscosity to entropy density ratio of the medium; see, e.g., [5] and references therein. In addition, probes of the medium that do not interact strongly are of great interest, since they escape largely unscathed once produced. In particular, the rate at which photons are emitted by the QGP is a classic—though challenging—observable in heavy-ion experiments [6]. Direct photons with a transverse

momentum below 2 GeV are found to admit an exponential spectrum, and models assuming the formation of the QGP are consistent with these measurements [7,8]. The production of weakly interacting particles by the QGP is also an important issue in early universe cosmology, for instance, in models which propose a keV-scale sterile neutrino as a dark matter candidate [9,10].

In this paper, we address the rate of photon emission from the QGP via lattice QCD simulations. One motivation to perform the calculation is that the rate vanishes in the limit of noninteracting quarks and gluons; therefore, it is a measure of the strength of their interactions. Second, direct photons emitted in heavy-ion collisions have been found to exhibit an unexpectedly large central value of elliptic flow [11,12]—albeit with significant uncertainty, therefore addressing their thermal production rate non-perturbatively can contribute to resolving the issue. Third, a controlled calculation of the photon rate paves the way for calculating the production of other particles, such as lepton pairs—relevant in heavy-ion phenomenology—or sterile neutrinos—relevant for validating or ruling out a dark matter candidate.

The main computational difficulty stems from the production of weakly interacting particles being a real-time process, which is accessible from the Matsubara path integral formalism implemented in lattice QCD only via an analytic continuation [13]. Numerically, the latter amounts to a poorly conditioned inverse problem discussed below.

II. THEORY BACKGROUND

We consider the full set of spectral functions of the electromagnetic current[1] $V^\mu = \sum_{f=u,d,s,...} Q_f \bar{\psi}_f \gamma^\mu \psi_f$,

$$\rho^{\mu\nu}(\omega, \vec{k}) = \int d^4 x e^{i(\omega x^0 - \vec{k}\cdot\vec{x})} \text{Tr}\left\{ \frac{e^{-\beta H}}{Z(\beta)} [V^\mu(x), V^\nu(0)^\dagger] \right\}. \quad (1)$$

For any four-vector u^μ, the form $u_\mu^\dagger \rho^{\mu\nu}(\omega, \vec{k}) u_\nu / \omega$ is real and non-negative; for u^μ real, it is also even in ω. Current conservation leads to $\omega^2 \rho^{00}(\omega, \vec{k}) = k^i k^j \rho^{ij}(\omega, \vec{k})$, implying that[2] $(\hat{k}^i \hat{k}^j \rho^{ij} - \rho^{00})/\omega$ has the same sign as $\mathcal{K}^2 \equiv \omega^2 - k^2$, and that it vanishes at lightlike kinematics, $\mathcal{K}^2 = 0$. It will be useful to consider the linear combination

$$\rho(\omega, k, \lambda) = (\delta^{ij} - \hat{k}^i \hat{k}^j)\rho^{ij} + \lambda(\hat{k}^i \hat{k}^j \rho^{ij} - \rho^{00}). \quad (2)$$

Defining the Euclidean correlator[3]

$$G_{\mu\nu}^E(x_0, \vec{k}) = \int d^3 x e^{-i\vec{k}\cdot\vec{x}} \langle V_\mu^E(x) V_\nu^E(0)^\dagger \rangle, \quad (3)$$

the corresponding linear combination

$$G(x_0, k, \lambda) = (\delta^{ij} - \hat{k}^i \hat{k}^j)G_{ij}^E + \lambda(\hat{k}^i \hat{k}^j G_{ij}^E - G_{00}^E) \quad (4)$$

admits the spectral representation

$$G(x_0, k, \lambda) = \int_0^\infty \frac{d\omega}{2\pi} \rho(\omega, k, \lambda) \frac{\cosh[\omega(\beta/2 - x_0)]}{\sinh(\beta\omega/2)}. \quad (5)$$

The production rate of dileptons with invariant mass squared equal to $\mathcal{K}^2$, which occurs via a timelike photon, is proportional to $\rho(\omega, k, 1)$ [14]. An interpretation of the spectral function for negative virtualities is provided in the Supplemental Material [15]. To leading order in the fine-structure constant $\alpha = e^2/(4\pi)$, the differential photon rate per unit volume of plasma can be written as

$$d\Gamma(k) = e^2 \frac{d^3 k}{(2\pi)^3 2k} \frac{\rho(k, k, \lambda)}{e^{\beta k} - 1} \quad (6)$$

and does not depend on λ. Given our goal of computing the photon rate, we choose $\lambda = -2$, because as a combined consequence of current conservation and Lorentz

---

[1] The Minkowski-space Dirac matrices satisfy $\{\gamma^\mu, \gamma^\nu\} = 2g^{\mu\nu}$ with $g^{\mu\nu} = \text{diag}(1, -1, -1, -1)$. Also, time evolution in Eq. (1) is Minkowskian, $V^\mu(t, \vec{x}) \equiv e^{-i(\vec{P}\cdot\vec{x} - Ht)} V^\mu(0, \vec{0}) e^{i(\vec{P}\cdot\vec{x} - Ht)}$.

[2] We use the notation $k \equiv |\vec{k}|$ and $\hat{k}^i = \frac{k^i}{k}$.

[3] The Euclidean current is defined by $V_\mu^E \equiv \sum_f Q_f \bar{\psi}_f \gamma_\mu^E \psi_f$, with $\{\gamma_\mu^E, \gamma_\nu^E\} = 2\delta_{\mu\nu}$. Also, time evolution is Euclidean in Eq. (3), $V_\mu^E(x) = e^{x_0 H - i\vec{P}\cdot\vec{x}} V_\mu^E(0) e^{-x_0 H + i\vec{P}\cdot\vec{x}}$.

invariance, $\rho(\omega, k, -2)$ vanishes identically in the vacuum (at zero temperature). Since, in addition, $\rho(\omega, k = 0, -2)$ vanishes exactly for $\omega \neq 0$ due to charge conservation, we expect from the operator-product expansion

$$\rho(\omega, k, -2) \propto k^2/\omega^4, \qquad \omega \gg \pi T, k. \quad (7)$$

This strong suppression in the ultraviolet implies a super-convergent sum rule for $\rho(\omega, k, -2)$,

$$\int_0^\infty d\omega\, \omega\, \rho(\omega, k, -2) = 0. \quad (8)$$

Spectral positivity implies that $\rho(\omega, k, -2)/\omega$ is non-negative for $\mathcal{K}^2 < 0$, and it must become negative for $\mathcal{K}^2 > 0$ in order to satisfy the sum rule (8).

In the infrared limit, the hydrodynamic prediction for $\rho(\omega, k, -2)$ reads

$$\rho(\omega, k, -2)/\omega \approx \frac{4\chi_s D k^2}{\omega^2 + (D k^2)^2} \qquad \omega, k \ll D^{-1}, \quad (9)$$

where D is the diffusion coefficient and $\chi_s \equiv \beta G^{00}(x_0, \vec{0})$ the static susceptibility. Therefore, following [18], we define the effective diffusion coefficient

$$D_{\text{eff}}(k) \equiv \frac{\rho(\omega = k, k, \lambda)}{4\chi_s k}, \quad (10)$$

which is proportional to the photon rate and tends to D in the limit $k \to 0$. In the weak-coupling regime, results at order g^2 have recently become available for general (ω, k) [19,20]. The photon rate itself has been obtained at order g^3 in [21].

From here on, we set $\lambda = -2$ and omit the last argument of $\rho(\omega, k, \lambda)$ and $G(\omega, k, \lambda)$.

III. THE LATTICE CALCULATION

We use lattice QCD with an isospin doublet of $O(a)$ improved Wilson fermions at a temperature of $T = 254$ MeV; the details of the lattice action can be found in [22] and references therein. Table I lists our ensembles, which allow us to take the continuum limit at a fixed temperature. All but the finest ensemble have a renormalized quark mass of $m^{\overline{\text{MS}}} \simeq 13$ MeV in the $\overline{\text{MS}}$ scheme at a renormalization scale of $\mu = 2$ GeV; on the finest ensemble, we have $m^{\overline{\text{MS}}} \simeq 16$ MeV. Quark-mass effects, which are suppressed by $(m/T)^2$ in the chirally symmetric phase, are therefore expected to be negligible. The ensembles F7, O7, and X7 were generated using the MP-HMC algorithm [23] in the implementation described in Ref. [24] based on the DD-HMC package [25], while ensemble W7 was generated using twisted-mass Hasenbusch frequency splitting in the version 1.6 of

TABLE I. Simulations at a fixed temperature of $T = (254 \pm 5)$ MeV and fixed aspect ratio $TL = 4$. For orientation, the transition temperature is about 211 MeV [28]. The number of point sources per configuration is 16 in all cases. The autocorrelation time of the squared topological charge defined at gradient-flow time [29] $\bar{t} = \beta^2/80$ is given in molecular-dynamics units (MDUs).

Label	$(6/g_0^2, \kappa)$	$1/(aT)$	N_{conf}	$\frac{\text{MDUs}}{\text{conf}}$	$\tau_{\text{int}}[Q^2(\bar{t})]$
F7	$(5.3, 0.13638)$	12	482	20	11.3(15)
O7	$(5.5, 0.13671)$	16	305	20	19(5)
W7	$(5.685727, 0.136684)$	20	1566	8	81(23)
X7	$(5.827160, 0.136544)$	24	511	10	490(230)

openQCD [26,27]. The ensembles labeled F7 and O7 have bare parameters identical to the zero-temperature F7 and O7 ensembles described in [22], for which the pion mass is 269 MeV.

We compute the correlator $G(x_0, k)$ of the isovector current $\frac{1}{\sqrt{2}} \bar{\psi} \gamma_\mu \tau^3 \psi$, which consists of a single connected Wick contraction.[4] The corresponding static susceptibility amounts to $G(x_0, 0)/(2T^3) = \chi_s/T^2 = 0.880(9)_{\text{stat}}(8)_{\text{syst}}$ in the continuum limit, where the systematic error reflects the dependence on using different prescriptions for the renormalization of the local vector current. We employ the local and the conserved vector currents, resulting in four discretizations of $G(x_0, k)$, and perform a constrained simultaneous continuum extrapolation. We have computed the leading-order perturbative lattice predictions, so that we are able to correct for the corresponding cutoff effects affecting our Monte Carlo data. To avoid incurring large cutoff effects at short distances, we omit data points for $x_0 < x_0^{\text{min}}$, where $x_0^{\text{min}} = \beta/4$ is our default value. We thus have data points for $G(x_0, k)$ at $x_0^{(i)} = \frac{i}{24} \cdot \beta$, $i \in \{6, 7, 8, 9, 10, 11, 12\}$. Given the high accuracy of the data, we are led to leave out the coarsest ensemble from the continuum limit, which leaves us with three lattice spacings for the linear extrapolation in a^2. The relative statistical precision of the continuum correlator is one to two permille. It is well known that the topological charge Q acquires a long autocorrelation time at small lattice spacings, and our simulations confirm this effect. However, we have found the dependence of the vector correlator of interest on $|Q|$ to be at most at the 3% level. Therefore, the vector correlator only suffers a modest increase in uncertainty from this algorithmic difficulty.

---

[4]In order to keep the notation concise, we do not explicitly distinguish between the quantities derived from the isovector and from the electromagnetic current. To obtain the photon rate from our results for $D_{\text{eff}}(k)$, we use Eq. (6) with $\rho(k, k) = 4k D_{\text{eff}}(k) \cdot \chi_s[Q_f]$ in the approximation $\chi_s[Q_f] \simeq C_{\text{em}} \cdot \chi_s[\text{isovector}]$, with $C_{\text{em}} = \sum_{f=u,d,s} Q_f^2 = 2/3$.

IV. ANALYSIS OF THE SPECTRAL FUNCTION

To obtain a global picture of the spectral function without committing to any specific functional form, in [30] we applied the Backus-Gilbert method to our data. The results confirm the theoretical expectation that most of the spectral weight is contained in the spacelike region $\omega^2 < k^2$.

A second method [30], that we now pursue further, consists in applying an explicit fit ansatz for the spectral function,

$$\rho(\omega, k) = \frac{A(1 + B\omega^2)\tanh(\omega\beta/2)}{[(\omega - \omega_0)^2 + b^2][(\omega + \omega_0)^2 + b^2][\omega^2 + a^2]}. \tag{11}$$

It satisfies the expected large-ω behavior (7), and, for given (a, b, ω_0), we always adjust B in such a way that the sum rule (8) is satisfied. We impose physically motivated lower bounds on a^2 and b^2. Our analysis treats the data at several momenta within one "group" simultaneously, assuming a locally affine dependence of the parameters (a, b, ω_0) on k^γ with either $\gamma = 1$ or 2. There are thus six nonlinear model parameters. We have performed scans over these six parameters, recording their $D_{\text{eff}}(k)$ and χ^2 values, and requiring a p value greater than 0.32 for a set of parameters to be considered acceptable. In evaluating the χ^2, we use a moderately regulated covariance matrix, which largely explains the smaller-than-usual set of χ^2 values we obtain. More details on our fitting procedures can be found in the Supplemental Material [15].

Before describing our results for $D_{\text{eff}}(k)$, we briefly present the outcome of our procedure when applied to mock Euclidean data generated from known spectral functions. For these tests, we have used the spectral functions of noninteracting quarks as well as those of the strongly coupled super Yang-Mills (SYM) theory [31]. In order to be realistic, we reuse the covariance matrix of our lattice QCD data, rescaled so as to achieve the same relative error on the correlator. In both cases, we find that the correct value of $D_{\text{eff}}(k)$ is one of those having a p value above 0.32. The output spectral functions yielding the highest p value tend to have a somewhat larger value of $D_{\text{eff}}(k)$.

Our final results for the $D_{\text{eff}}(k)$ values yielding a p value above 0.32 for the QCD correlator at $T = 254$ MeV are displayed in Fig. 1. We show results for both the linear and the quadratic dependence on k, $\gamma = 1$ and 2. We observe that for the third momentum group, containing momenta above 1.0 GeV, the values of $D_{\text{eff}}(k) \cdot$ GeV cover the interval [0, 0.7] and are thus compatible both with the leading-order weak-coupling prediction [32] and the strongly coupled SYM prediction [31], which lie between 0.3 and 0.5. Moreover, the weak-coupling prediction is among those values with the highest p value. In the second
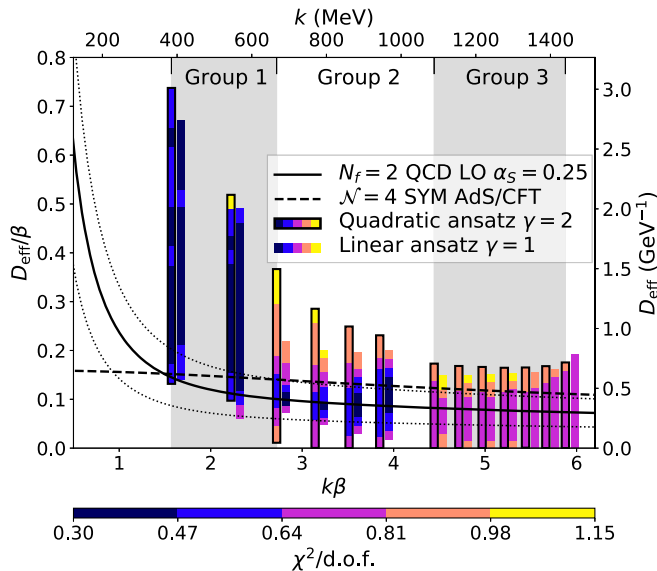
FIG. 1. Lattice results for the effective diffusion coefficient $D_{\mathrm{eff}}(k)$, defined by Eqs. (6) and (10). The color-coded vertical bars represent those values of D_{eff} for which a spectral function of the form (11) exists that has a p value above 0.32. The colors indicate the smallest $\chi^2/\mathrm{d.o.f.}$ found for a given value of D_{eff}. Shaded areas identify the momentum groups that are fitted simultaneously; for each momentum, results are shown both for the $\gamma = 1$ and $\gamma = 2$ parametrizations of the k dependence of the nonlinear parameters. Analytical results from perturbative QCD [32] (with a 40% uncertainty band [21]) and from the strong-coupling limit of $\mathcal{N} = 4$ SYM theory [31] are shown for comparison.

momentum group, the range of acceptable $D_{\mathrm{eff}}(k)$ values covers a range up to about twice the strongly coupled SYM value (for the ansatz quadratic in k), while again the weak-coupling prediction has one of the highest p values. In the group of smallest momenta, the lattice data lose sensitivity to the photon rate. Particularly, the data do not exclude large values of $D_{\mathrm{eff}}(k)$. Finally, we remark that our fits yield a strong correlation between the values of $D_{\mathrm{eff}}(k)$ at successive k [33].

It is instructive to look at the full frequency dependence of the spectral functions which describe the QCD correlators. In Fig. 2, as representative examples for the three spatial momenta $k = (0.40, 0.98, 1.49)$ GeV, we show spectral functions that correspond to the upper and lower ends of the $D_{\mathrm{eff}}(k)$ ranges shown in Fig. 1. We also display the spectral function leading to the smallest χ^2, and for comparison, the spectral functions of noninteracting quarks as well as those of the strongly coupled SYM theory. For the second and third momenta, we observe that all three spectral functions describing the QCD correlators exhibit a smooth behavior for $\omega^2 < k^2$ and admit a maximum near the point $\omega = k$, its precise location being tightly linked to the value of $D_{\mathrm{eff}}(k)$ and hence to the photon emission rate.
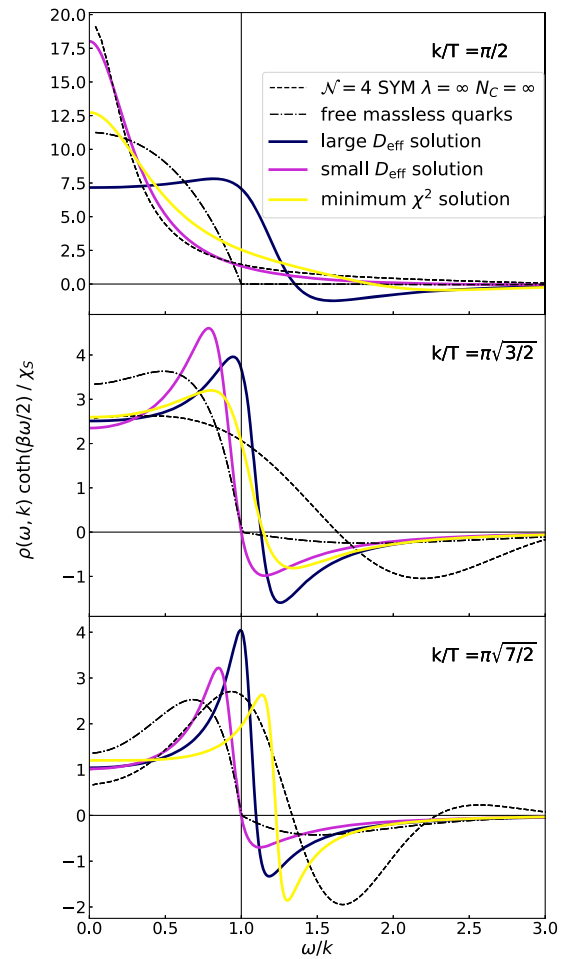

FIG. 2. Representative spectral functions obtained from lattice QCD data for three different spatial momenta. They are compared to the spectral functions of noninteracting quarks and of the strongly coupled SYM theory.

V. CONCLUSION

Using lattice simulations in the quark-gluon plasma phase of QCD with two dynamical quark flavors at a temperature of 254 MeV, we have computed one particularly ultraviolet-soft component of the polarization tensor in the continuum limit. This component determines the photon emission rate from the medium via analytic continuation; in practice, however, one is faced with the inverse problem [Eq. (5)] for the spectral function. We explored exhaustively the parameter space of the Padé-form spectral functions in Eq. (11). The photon rate is given, up to kinematical factors, by the spectral function at photon kinematics, $\omega = k$, and normalizing this quantity by the well-determined static charge susceptibility, one obtains the effective (momentum-dependent) diffusion coefficient. The latter is only mildly sensitive to the number of charged degrees of freedom in the plasma: the strongly coupled SYM and the weak-coupling QCD predictions are comparable and slowly varying functions of k for $k \geq \pi T$.

Within the explored family of spectral functions, we determined which values of this coefficient are compatible with the Euclidean data; our result is displayed in Fig. 1. We have validated our handling of the inverse problem and the associated uncertainties by applying the same procedure to the strongly coupled SYM theory and to QCD at zero coupling, which represent extreme opposite caricatures of the quark-gluon plasma. Our results imply nonperturbative constraints on the possible rate of photon emission from the QGP at a temperature typical for the strongly interacting system created in heavy-ion collision experiments. For $k \geq \pi T$, we largely confirm the weak-coupling predictions, in spite of the relatively low temperature of 254 MeV. Specifically, we quote the thermal photon emissivities

$$\frac{d\Gamma(k) \cdot (10 \text{ fm})^4}{d(k/(0.2 \text{ GeV}))} = \begin{cases} 4.4^{+6.2}_{-1.9} & k = 0.80 \text{ GeV}, \\ 1.5^{+2.1}_{-1.5} & k = 1.20 \text{ GeV}, \end{cases} \quad (12)$$

where the asymmetric uncertainties are determined from the extent of the vertical bars of the $\gamma = 1$ fits in Fig. 1 and reflect both the statistical and the systematic uncertainty associated with the inverse problem. Our results are also in good agreement with those of a previous lattice calculation performed in the quenched approximation [18].

What are the implications of our findings for predictions of the direct photon yield and spectrum in heavy-ion collisions at RHIC or the LHC? In hydrodynamic studies [34,35] thereof, the photon emissivity of thermalized quark-gluon plasma is one of the several key ingredients. Given that the leading perturbative rate of photon emission was used in the latter publications, and that our calculation largely confirms this rate, the implication is that it consolidates these predictions. In regard to the observation of an unexpectedly large elliptic flow of direct photons [11,12], it would be very interesting to repeat the present calculation at a temperature in the crossover region, in order to see whether the photon emissivity is substantially higher than an interpolation of QGP and hadronic-phase emissivities. That a higher fraction of direct photons could be produced in the later, cooler stages of the heavy-ion collision has been proposed as a possible explanation of the observed photon elliptic flow [36].

As a study based on lattice correlators computed for noninteracting quarks shows, adding data points at shorter Euclidean time significantly enhances the ability of the data to exclude large values of D_{eff}, particularly at low photon momenta. This calls for even finer lattices to be used, which represents a challenge in view of the large lattice sizes required and the long associated autocorrelation times. We finally remark that a different strategy has also recently been proposed for lattice QCD to compute the photon rate using a dispersion relation at fixed, vanishing virtuality [37].

[1] S. Borsanyi, Z. Fodor, C. Hoelbling, S. D. Katz, S. Krieg, C. Ratti, and K. K. Szabó (Wuppertal-Budapest Collaboration), J. High Energy Phys. 09 (2010) 073.

[2] A. Bazavov, T. Bhattacharya, M. Cheng, C. DeTar, H. Ding *et al.*, Phys. Rev. D **85**, 054503 (2012).

[3] T. Bhattacharya, M. I. Buchoff, N. H. Christ, H. T. Ding, R. Gupta *et al.*, Phys. Rev. Lett. **113**, 082001 (2014).

[4] P. Braun-Munzinger, V. Koch, T. Schaefer, and J. Stachel, Phys. Rep. **621**, 76 (2016).

[5] C. Shen and U. Heinz, Nucl. Phys. News **25**, 6 (2015).

[6] G. David, Rep. Prog. Phys. **83**, 046301 (2020).

[7] A. Adare *et al.* (PHENIX Collaboration), Phys. Rev. C **91**, 064904 (2015).

[8] J. Adam *et al.* (ALICE Collaboration), Phys. Lett. B **754,** 235 (2016).

[9] T. Asaka, M. Laine, and M. Shaposhnikov, J. High Energy Phys. 06 (2006) 053.

[10] T. Asaka, M. Laine, and M. Shaposhnikov, J. High Energy Phys. 01 (2007) 091.

[11] A. Adare *et al.* (PHENIX Collaboration), Phys. Rev. C **94,** 064901 (2016).

[12] S. Acharya *et al.* (ALICE Collaboration), Phys. Lett. B **789,** 308 (2019).

[13] H. B. Meyer, Eur. Phys. J. A **47**, 86 (2011).

[14] L. D. McLerran and T. Toimela, Phys. Rev. D **31**, 545 (1985).

[15] See Supplemental Material at http://link.aps.org/supplemental/10.1103/PhysRevD.102.091501 for a physics interpretation of the spectral function, as well as details of the continuum extrapolation and of the analysis of the spectral function, which includes Refs. [16,17].

[16] P. Arnold, G. D. Moore, and L. G. Yaffe, J. High Energy Phys. 05 (2003) 051.

[17] H.-T. Ding, O. Kaczmarek, and F. Meyer, Phys. Rev. D **94,** 034504 (2016).

[18] J. Ghiglieri, O. Kaczmarek, M. Laine, and F. Meyer, Phys. Rev. D **94,** 016005 (2016).

[19] M. Laine, J. High Energy Phys. 11 (2013) 120.

[20] G. Jackson and M. Laine, J. High Energy Phys. 11 (2019) 144.

[21] J. Ghiglieri, J. Hong, A. Kurkela, E. Lu, G. D. Moore, and D. Teaney, J. High Energy Phys. 05 (2013) 010.

[22] P. Fritzsch, F. Knechtli, B. Leder, M. Marinkovic, S. Schaefer, R. Sommer, and F. Virotta (ALPHA Collaboration), Nucl. Phys. **B865,** 397 (2012).

[23] M. Hasenbusch, Phys. Lett. B **519,** 177 (2001).

[24] M. Marinkovic and S. Schaefer, Proc. Sci., LATTICE2010 (**2010**) 031.

[25] http://luscher.web.cern.ch/luscher/DD-HMC/index.html (2010).

[26] M. Lüscher and S. Schaefer, Comput. Phys. Commun. **184,** 519 (2013).

[27] http://luscher.web.cern.ch/luscher/openQCD (2013).

[28] B. B. Brandt, A. Francis, H. B. Meyer, O. Philipsen, D. Robaina, and H. Wittig, J. High Energy Phys. 12 (2016) 158.

[29] M. Lüscher, J. High Energy Phys. 08 (2010) 071.

[30] B. B. Brandt, A. Francis, T. Harris, H. B. Meyer, and A. Steinberg, EPJ Web Conf. **175,** 07044 (2018).

[31] S. Caron-Huot, P. Kovtun, G. D. Moore, A. Starinets, and L. G. Yaffe, J. High Energy Phys. 12 (2006) 015.

[32] P. B. Arnold, G. D. Moore, and L. G. Yaffe, J. High Energy Phys. 12 (2001) 009.

[33] B. B. Brandt, M. Cè, A. Francis, T. Harris, H. B. Meyer, A. Steinberg, and A. Toniato, Proc. Sci., LATTICE2019 (2019) 225.

[34] C. Shen, U. W. Heinz, J.-F. Paquet, and C. Gale, Phys. Rev. C **89,** 044910 (2014).

[35] J.-F. Paquet, C. Shen, G. S. Denicol, M. Luzum, B. Schenke, S. Jeon, and C. Gale, Phys. Rev. C **93,** 044906 (2016).

[36] H. van Hees, C. Gale, and R. Rapp, Phys. Rev. C **84,** 054906 (2011).

[37] H. B. Meyer, Eur. Phys. J. A **54,** 192 (2018).